

Supporting Information

A facile, low-cost bimetallic iron-nickel MOF nanozyme-propelled ratiometric fluorescent sensor for highly sensitive and selective uric acid detection and its smartphone application

Jiawen Han,^a Yuwei Zhang,^a Xujuan Lv,^a Daoqing Fan^{*ab} and Shaojun Dong^b

^a Laboratory for Marine Drugs and Bioproducts, National Laboratory for Marine Science and Technology; Key Laboratory of Marine Drugs, Ministry of Education, School of Medicine and Pharmacy, Ocean University of China; Qingdao, Shandong, 266003, China.

^b State Key Laboratory of Electroanalytical Chemistry, Changchun Institute of Applied Chemistry, Chinese Academy of Sciences, Changchun, 130022, China.

Email: fdq9688@ouc.edu.cn; dqfan93@163.com.

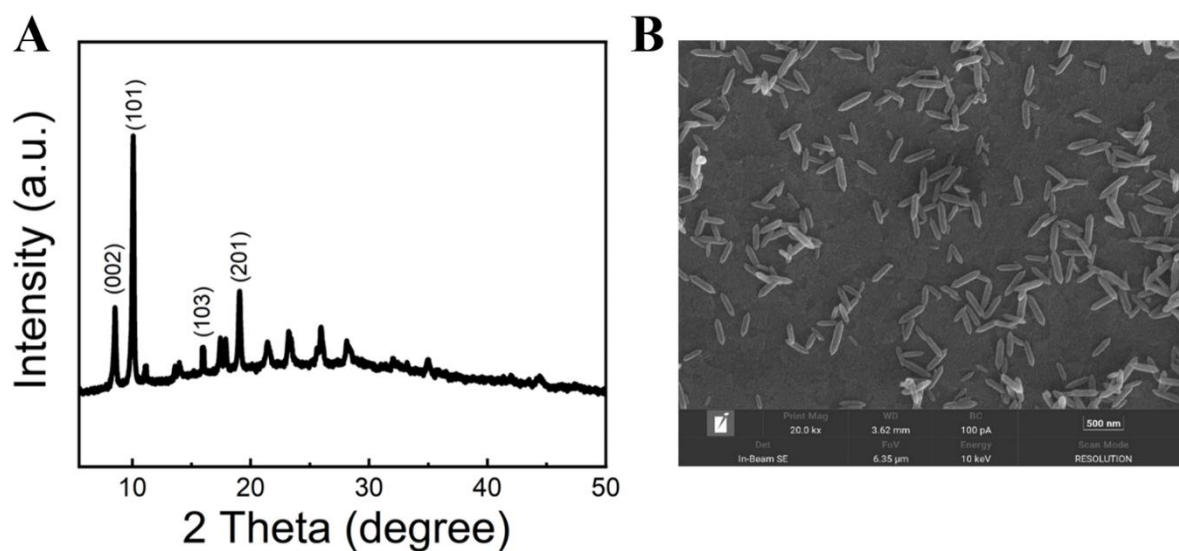


Fig. S1. (A) XRD pattern of Fe-MOF-NH₂. Fe-MOF-NH₂ exhibited four major peaks at 8°, 10°, 16° and 19° which correspond to (002), (101), (103) and (201) peaks of Fe-MOF-NH₂ phases, respectively. (B) SEM image of Fe-MOF-NH₂ at the scale of 500 nm.

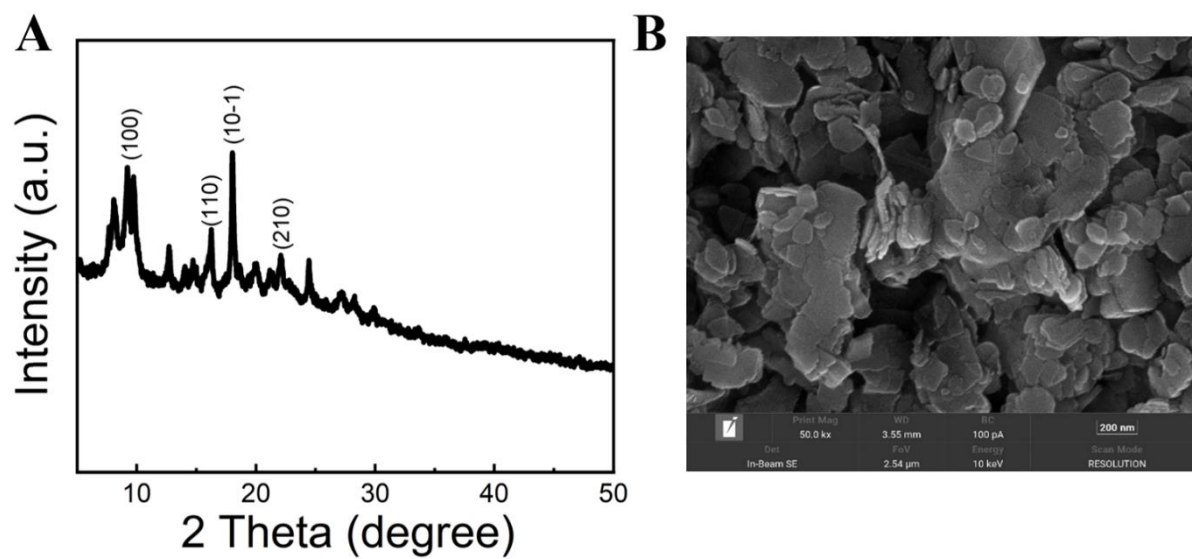


Fig. S2. (A) XRD pattern of Ni-MOF-NH₂. Ni-MOF-NH₂ showed four major peaks at 10°, 16°, 18° and 22° which correspond to (100), (110), (101) and (210) peaks of Ni-MOF-NH₂ phases, respectively. (B) SEM image of Ni-MOF-NH₂ at 200 nm.

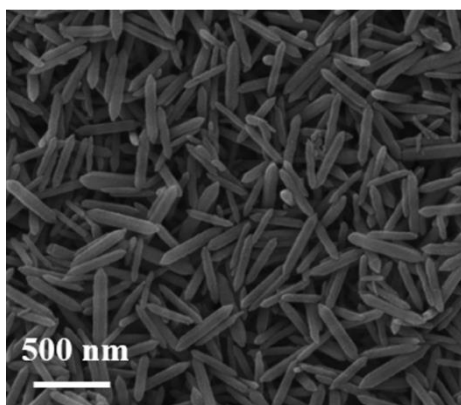


Fig. S3. SEM image of $\text{Fe}_3\text{Ni-MOF-NH}_2$ at 500 nm scale.

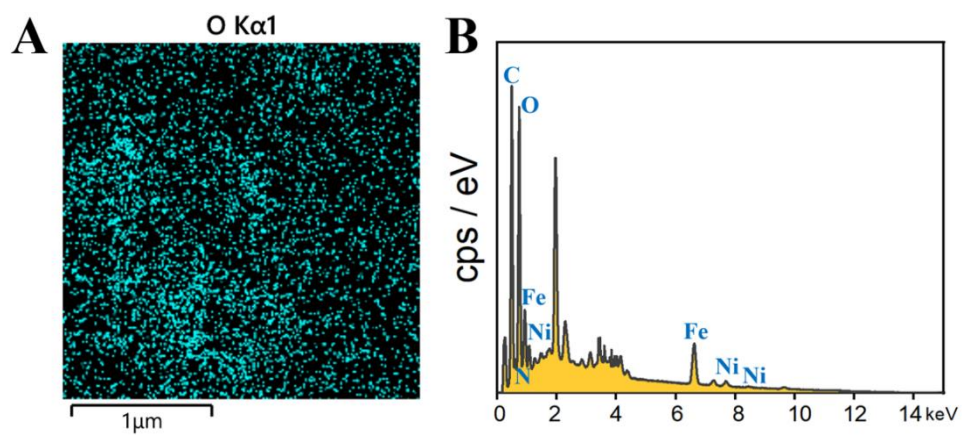


Fig. S4. (A) SEM elemental mapping image of oxygen element. (B) Map Sum Spectrum of Fe₃Ni-MOF-NH₂.

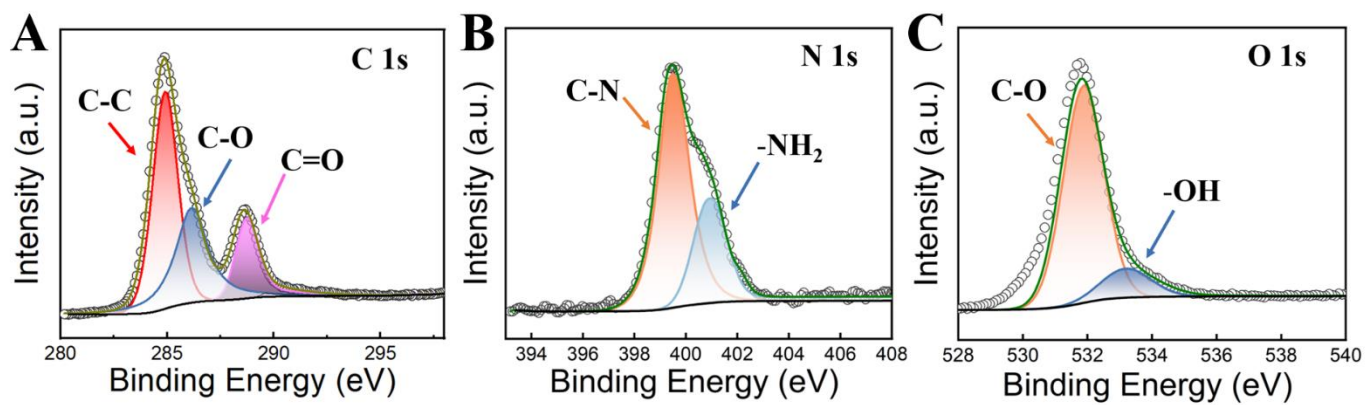


Fig. S5. (A) High-resolution XPS spectra of C 1s, N 1s (B) and O 1s (C).

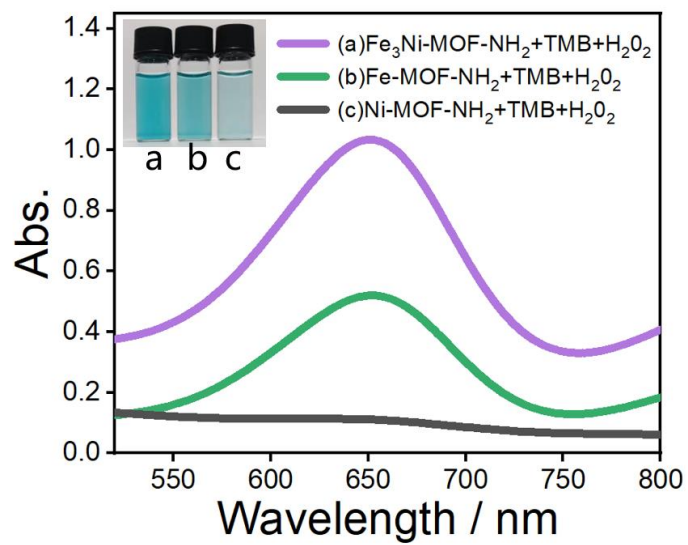


Fig. S6. Comparison of peroxidase (POD)-like catalytic activity of Fe₃Ni-MOF-NH₂, Fe-MOF-NH₂ and Ni-MOF-NH₂, and the corresponding UV-visible spectra (7 μ L Fe_xNi_y-MOF-NH₂, 0.2 mM TMB and 10 mM H₂O₂ were used).

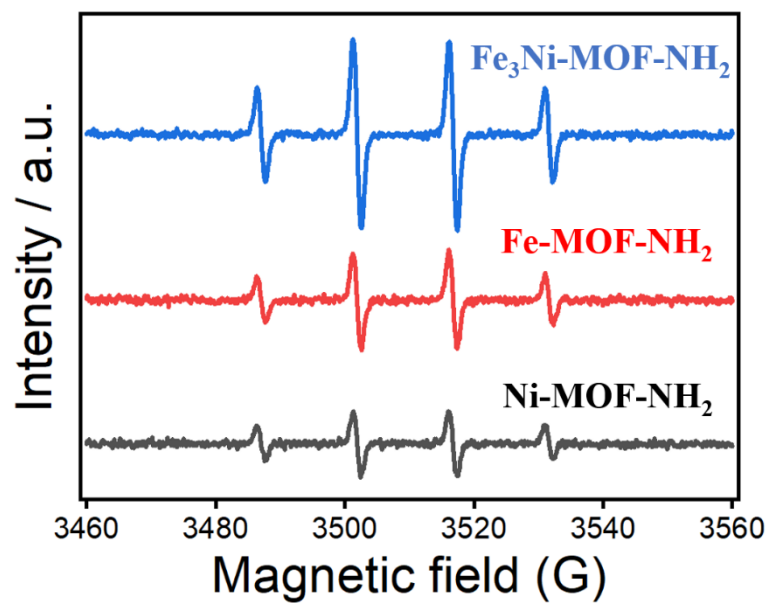


Fig. S7. EPR spectra of the DMPO/•OH spin adduct of $\text{Fe}_3\text{Ni-MOF-NH}_2$, Fe-MOF-NH_2 and Ni-MOF-NH_2 .

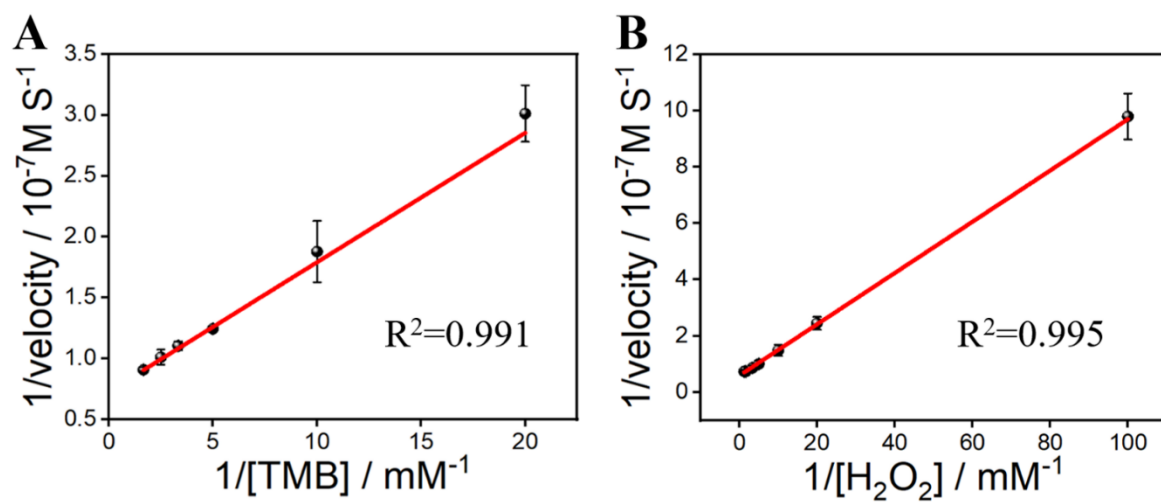


Fig. S8. (A) Lineweaver-Burk double reciprocal plots of $\text{Fe}_3\text{Ni-MOF-NH}_2$ for TMB and (B) H_2O_2 .

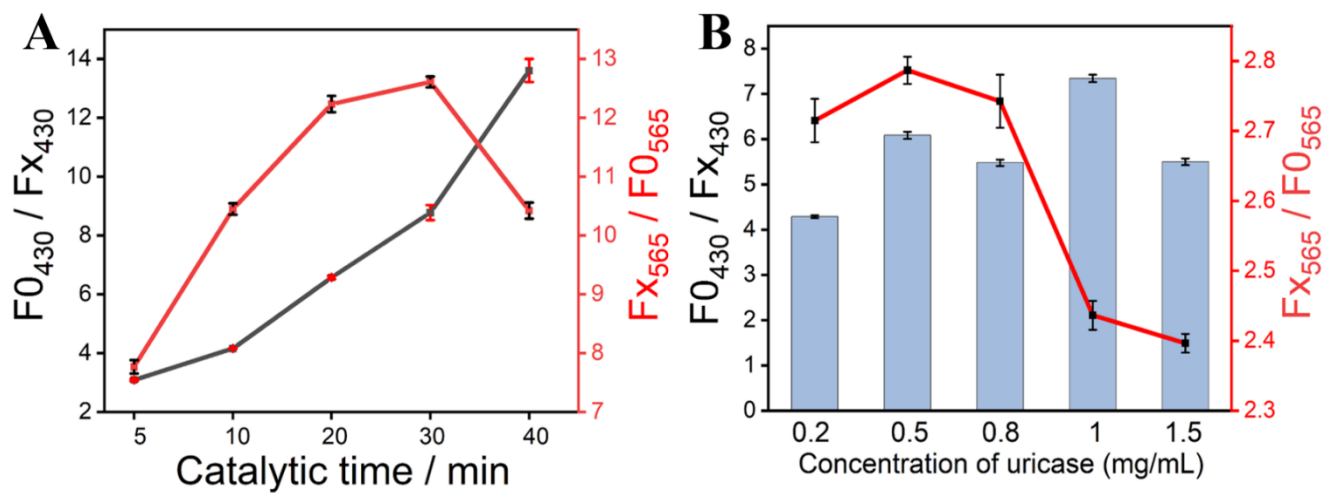


Fig. S9. (A) Optimization of catalytic time. (B) Optimization of uricase's concentration.

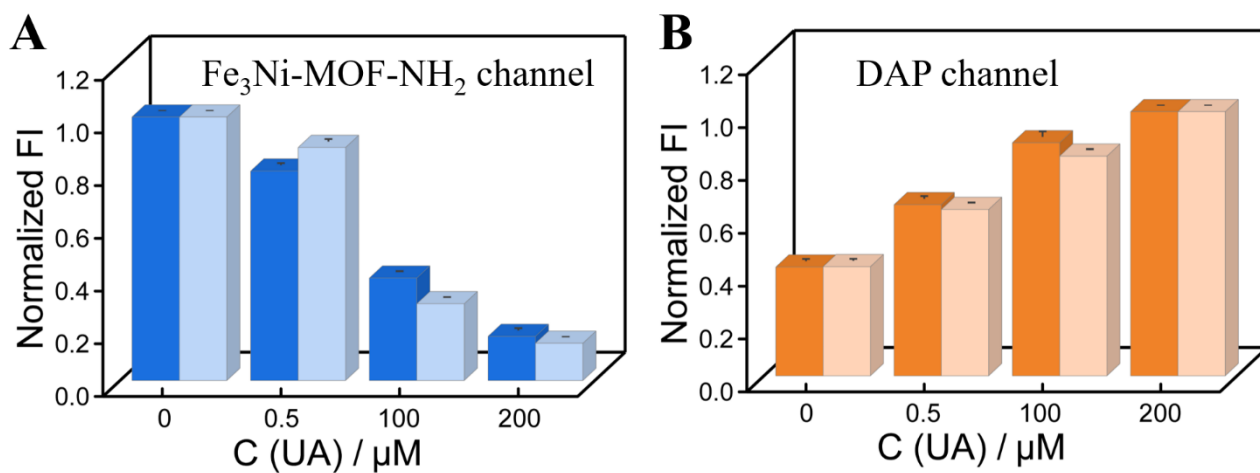


Fig. S10. (A) 3D normalized fluorescent column bars of $\text{Fe}_3\text{Ni-MOF-NH}_2$ with different concentrations of UA in a 2-month storage period at 4°C (bright-blue columns: day 0, pale-blue: after 2 months). (B) 3D normalized fluorescent column bars of DAP with different concentrations of UA in a 2-month storage period at 4°C (bright-orange columns: day 0, pale-orange: after 2 months).

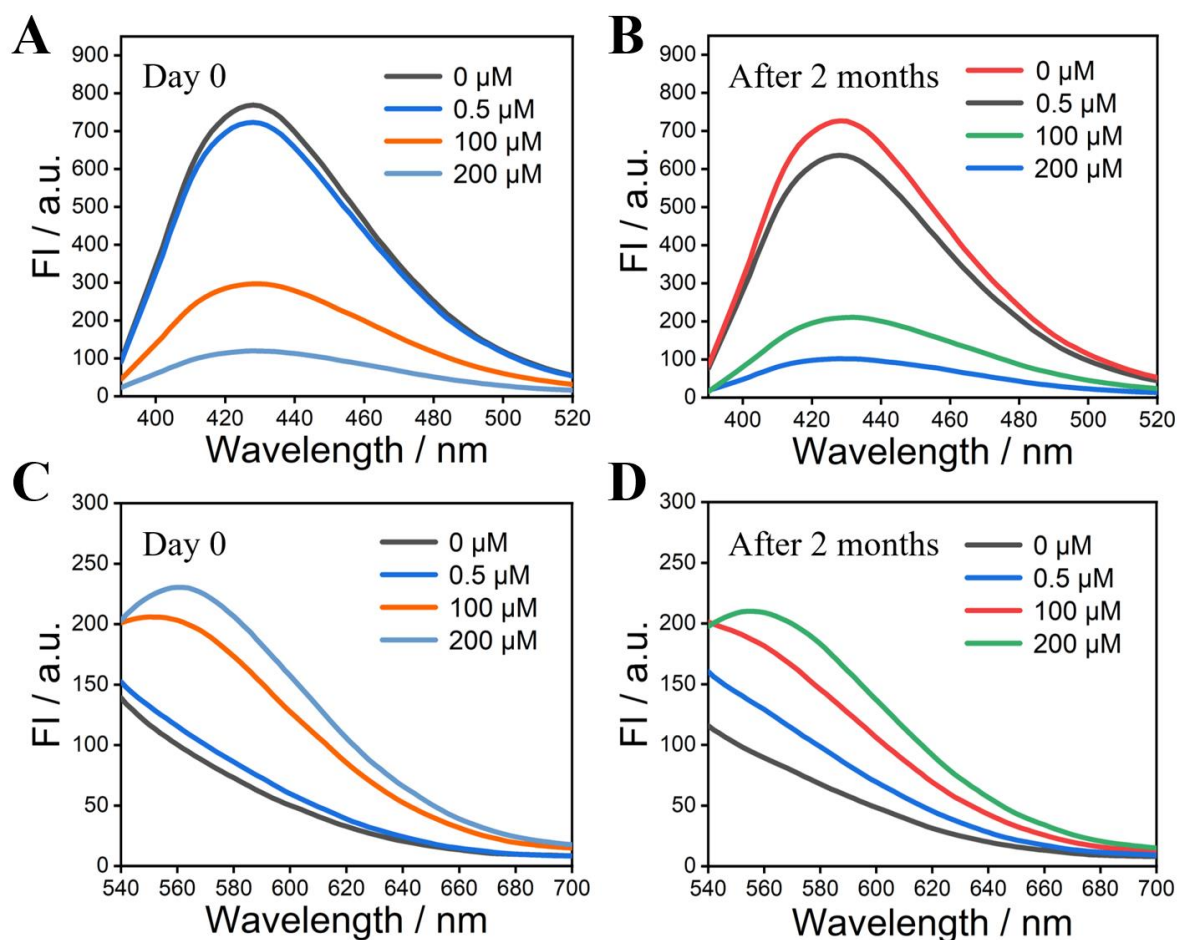


Fig. S11. (A) Fluorescence spectra of Fe₃Ni-MOF-NH₂ with various concentrations of UA on day 0. (B) Fluorescence spectra of Fe₃Ni-MOF-NH₂ after 2 months with same concentrations of UA as on day 0. (C) Fluorescence spectra of DAP with various concentrations of UA on day 0. (D) Fluorescence spectra of DAP after 2 months with various concentrations of UA.

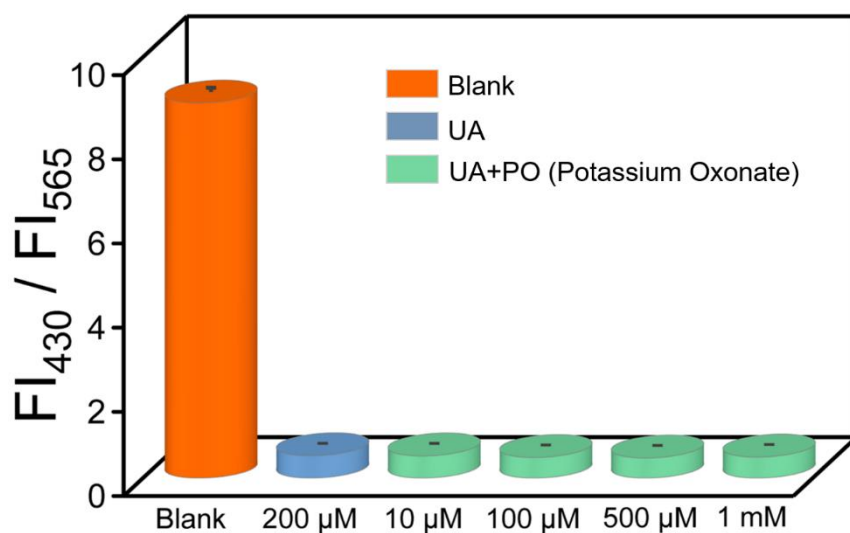


Fig. S12. 3D normalized ratiometric fluorescent column bars of the platform in the absence and presence of PO (orange column: 0.5 mg/mL uricase, blue column: 0.5 mg/mL uricase + 200 μ M UA, green columns: 0.5 mg/mL uricase + 200 μ M UA + PO).

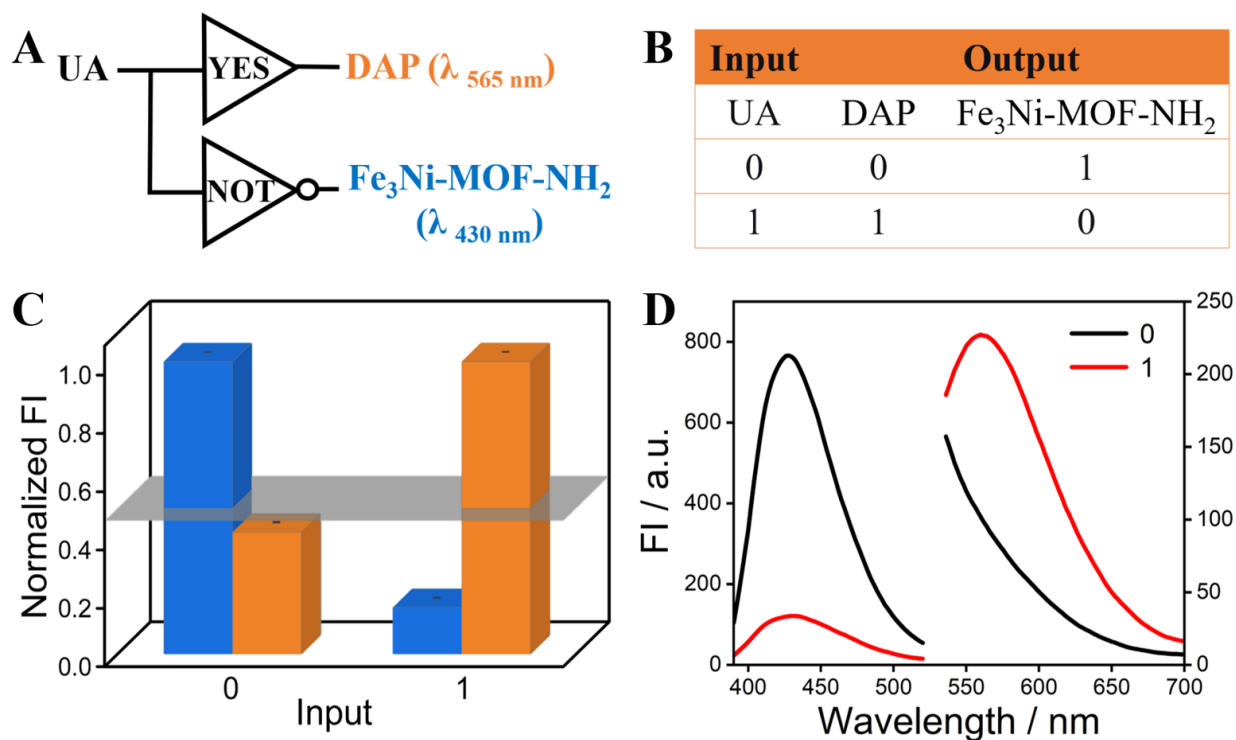


Fig. S13. (A) Equivalent logic symbol of YES[^]NOT logic pair. (B) Corresponding truth table of the YES[^]NOT logic pair. (C) 3D normalized fluorescent column bars of Fe₃Ni-MOF-NH₂ (blue columns) and that of DAP (orange columns) in the absence and presence of UA. (D) Fluorescence spectra of Fe₃Ni-MOF-NH₂ and DAP under different input combinations of YES[^]NOT logic pair.

Table S1. Comparison of kinetic parameters (K_m and V_{max}) of $Fe_3Ni-MOF-NH_2$ and HRP.

Catalyst	Substrate	K_m (mM)	V_{max} ($10^{-7} M \cdot s^{-1}$)	Ref.
$Fe_3Ni-MOF-NH_2$	TMB	0.1458	1.3727	This work
	H_2O_2	0.1532	1.6838	This work
HRP	TMB	0.434	1.00	(43)
	H_2O_2	3.70	0.871	(43)